Accepted Manuscript

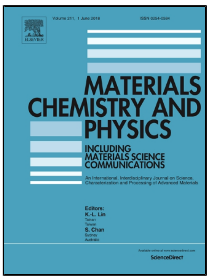

Formation of Nickel Nanoparticles and Magnetic Matrix in Nickel Phthalocyanine by Doping with Potassium.

Aram S. Manukyan, Leon A. Avakyan, Anna E. Elsukova, Yan V. Zubavichus, Sergey N. Sulyanov, Armen A. Mirzakhanyan, Natalia A. Kolpacheva, Marina Spasova, Armen N. Kocharian, Michael Farle, Lusegen A. Bugaev, Eduard G. Sharoyan

PII:	S0254-0584(18)30337-7
DOI:	10.1016/j.matchemphys.2018.04.068
Reference:	MAC 20563
To appear in:	*Materials Chemistry and Physics*
Received Date:	20 December 2016
Revised Date:	07 March 2018
Accepted Date:	21 April 2018

Please cite this article as: Aram S. Manukyan, Leon A. Avakyan, Anna E. Elsukova, Yan V. Zubavichus, Sergey N. Sulyanov, Armen A. Mirzakhanyan, Natalia A. Kolpacheva, Marina Spasova, Armen N. Kocharian, Michael Farle, Lusegen A. Bugaev, Eduard G. Sharoyan, Formation of Nickel Nanoparticles and Magnetic Matrix in Nickel Phthalocyanine by Doping with Potassium., *Materials Chemistry and Physics* (2018), doi: 10.1016/j.matchemphys.2018.04.068

Formation of Nickel Nanoparticles and Magnetic Matrix in Nickel Phthalocyanine by Doping with Potassium.

Aram S. Manukyan[a,*], Leon A. Avakyan[b], Anna E. Elsukova[c], Yan V. Zubavichus[d], Sergey N. Sulyanov[d], Armen A. Mirzakhanyan[a], Natalia A. Kolpacheva[b], Marina Spasova[c], Armen N. Kocharian[e], Michael Farle[c], Lusegen A. Bugaev[b], Eduard G. Sharoyan[a]

a) Institute for Physical Research, National Academy of Sciences of Armenia, Ashtarak 0203, Armenia
b) Department of Physics, Southern Federal University, Rostov-on-Don, 344090, Russia
c) Fakultät für Physik and Center for Nanointegration Duisburg-Essen (CeNIDE), Universität Duisburg-Essen, Lotharstr. 1, Duisburg D-47048, Germany
d) National Research Center "Kurchatov Institute", Moscow 123182, Russia
e) California State University, Los Angeles, CA, 90032, USA

** E-mail address: manukyan.ipr@gmail.com*

Abstract

A method for synthesis of nickel nanoparticles in a magnetic nickel phthalocyanine anions matrix has been developed. The method is based on intercalation of potassium atoms to the nickel phthalocyanine (NiPc) polycrystalline powder at 300°C. The structure of (K_2NiPc) was investigated by using high-resolution transmission electron microscopy (HRTEM), X-ray diffraction (XRD) and X-ray absorption fine structure (XAFS) spectroscopes. Magnetic properties were studied by SQUID magnetometry and magnetic resonances methods. It is revealed that the resultant compound contains of 1 wt% Ni nanoparticles with the average size of 15 nm. The measured values of the magnetization and absorption of the ferromagnetic resonance considerably exceed the magnetism which can be attributed to metallic Ni nanoparticles. The obtained results indicate the presence of room temperature molecular ferromagnetism caused by anionic molecules of NiPc.

Keywords: nickel nanoparticles, phthalocyanine matrix, molecular magnetism, magnetic resonances and magnetic properties, HRTEM, XRD and XAFS study

---

1. Introduction

Nanosized magnetic nanoparticles such as Fe, Co, Ni stabilized in metal-phthalocyanine (MPc) matrices are attracting attention because of their potential applications in optoelectronic devices organic semiconductors devices, etc [1-4]. Due to their strong absorption in the near infrared (NIR) region and

exceptional photophysical efficiencies, phthalocyanines are very promising agents for photodynamic therapy [5]. Recently, thin films of phthalocyanines doped with electrons attract a great interest in molecular spintronics, as well as in strongly correlated electronic systems [6].

The formation of nickel nanoparticles in phthalocyanine matrix was studied in [7] synthesized by co-deposition of metal and phthalocyanine vapors, but the obtained nanoparticles were oxidized after ten days exposition to air. Magnetic properties of metal-phthalocyanines doped with alkaline metals were investigated also earlier in papers [8-10]. It was shown that in some cases metal nanoparticles in MPc were formed depending on the doping conditions. However, the high concentrations of doping atoms did not allow to determine reliably the magnetic properties of the doped MPc matrix. Thus, the origin of the observed magnetic properties of the synthesized MPc samples doped with alkaline metals remains a challenging problem.

In our previous work [11], single domain Ni nanoparticles in carbon matrix have been prepared using solid-phase pyrolysis of nickel phthalocyanine and investigated. In the present paper, a gas-phase doping of NiPc with potassium at 300 °C was performed (Sec. 2). The obtained sample (K_2NiPc) demonstrates a room temperature ferromagnetism and is air stable. The structural characterization of this composite material was performed by the following methods: i) high resolution transmission electron microscopy (HRTEM) providing the real space images of the composites and X-ray diffraction (SI-XRD), which probes the long-range atomic structure (Sec.3.1), ii) Ni K-edge X-ray absorption fine structures (XAFS), which is very sensitive to the details of the local atomic structure around the absorbing Ni atom (Sec.3.2). The application of these complementary techniques enabled to reveal the presence of Ni nanoparticles in the intercalated matrix of NiPc. Magnetic properties of the sample were studied by SQUID-magnetometry, ferromagnetic and electron spin resonance (FMR, ESR) methods (Sec.3.3). The results of this study allowed conclude that the exhibited strong magnetic properties of (K_2NiPc) can be partly attributed to the formed Ni nanoparticles and partly – to the anionic molecules of NiPc formed under its doping with potassium.

2. Experimental

Initial nickel phthalocyanine powder samples were synthesized by Linstead method using phthalonitrile and corresponding nickel salts [12]. The synthesis products were purified by washing in acid and alkaline media consequently. After that the samples were twice sublimed in vacuum at 500-550 °C.

Nickel nanoparticles were produced by intercalation of heated up to 300 °C potassium vapor in the polycrystalline powder of NiPc. This method of gas-phase doping of phthalocyanines has been described in detail previously [8-10].

It is expected that the doping by alkaline atoms of MPc molecules dissolved in tetrahydrofuran or other solvent will lead to the reduction of MPc molecules [13-17]. In that case the step-by-step reduction of mono-, di-, tri- and tetra-anions of MPc takes place according the following scheme:

$$MPc + ne^- \rightarrow (MPc)^{n-}, \quad n = 1, 2, 3, 4. \tag{1}$$

The same scheme could be written for the process of doping of MPc in a solid phase:

$$MPc + xA \rightarrow A_xMPc, \quad 0 < x < 4. \tag{2}$$

However, the compounds obtained by the doping of monocrystals, polycrystals or thin films of MPc are significantly differ from the products of the liquid-phase synthesis. The main reason is that the doping of MPc in the solution takes place only in $(MPc)^{n-}$ anions with integer charge number $n = 1, 2, 3, 4$. In contrast, the doping of solid phthalocyanines can occur at fractional charges ($n = 1.5, 2.5,$ etc). Varying the concentration of dopant x, it is possible to obtain new compounds with different structural, electric and magnetic properties.

In the present work, the studied polycrystalline samples of NiPc where doped by potassium vapor resulting in K_xNiPc sample according the scheme:

$$NiPc + x\,K \leftrightarrow (K^+)_x(NiPc)^{x-} \tag{3}$$

where $0 < x < 3$. In the most cases the doping is not homogeneous and in the regions of high dopant concentrations ($x > 3$) the NiPc molecules can be destroyed with production of nickel atoms, which are diffusing and forming the nickel nanoparticles. Fresh K_xNiPc samples were annealed at 280 °C for 2 hours. After that the samples were washed with distilled water in order to remove the extra potassium atom. The elemental analysis performed by INCA-Energy 300 (Electron Dispersive Spectrometer) indicated that in the

resulted K_xNiPc sample the concentration of potassium x varies from 1 to 3 in different parts of the same sample. The average value of x in the sample is about 2, hereafter the sample will be referred as (K_2NiPc). It is important to mention that this sample is attracted by a weak permanent magnet.

The structural studies were performed by TEM, XRD and XAFS methods. The TEM micrographs were obtained on a high resolution transmission electron microscope FEI Tecnai F20.

The X-ray diffraction patterns of NiPc and (K_2NiPc) samples were measured at the "Structural Materials Science" beamline of the Kurchatov Synchrotron Radiation Source (Moscow, Russia). The electron storage ring Siberia-2 were operated at electron energy of 2.5 GeV with mean electron current of 100 mA. The diffraction measurements were performed in the transmission mode at a wavelength of 1.072 Å using a FujiFilm ImagePlate 2D detector. Ni K-edge XAFS spectra were measured at the same experimental station in the transmission mode utilizing a Si(111) channel-cut monochromator and two ionization chambers filled with appropriate N_2-Ar mixtures to provide 20% and 80% absorption for I_0 and I_t, respectively. The scanning steps were adjusted to $\delta E \sim 0.3$ eV and $\delta k \sim 0.05$ Å^{-1} in the XANES and EXAFS regions, respectively. The total acquisition time was about 30 min per spectrum.

The magnetic measurements were performed using a Quantum Design MPMS-XL5 SQUID-Magnetometer. The temperature was varied in a wide range from 7 to 300 K and the maximum available external magnetic field had value of 50000 Oe. Magnetic resonances spectra were measured in the same temperature range using X-band spectrometer JEOL-JES-PE-3X.

3. Results and discussion

3.1. TEM and STEM images, size distribution and XRD investigation

Figure 1(a) presents HRTEM image of (K_2NiPc) sample, where the darker spots corresponds to the nickel nanoparticles. The Figure 1(b) illustrates the size distribution of nickel nanoparticles in (K_2NiPc) sample, obtained by counting of 150 nanoparticles from several TEM-images. The solid line represents the fitting curve assuming a lognormal function, where the average size is 15 nm with standard deviation of $\sigma \approx 0.6$. The ordinate axis is normalized to $N_{max} = 45$. The presence of Ni nanoparticles in (K_2NiPc) matrix was confirmed

by High Angular Annular Dark Field – Scanning TEM (HAADF-STEM) imaging technique combined with EDX spectroscopy. Fig. 1(c) shows the HAADF-STEM image of a (K_2NiPc) sample. The areas with the bright contrast correspond to Ni nanoparticles as proved by EDX line scans (fig. 1(d)).

Figure 2 presents synchrotron radiation XRD patterns of pure NiPc, (K_2NiPc) and Ni-foil. The comparison shows that the two peaks in the region of large angles $2\theta > 30°$ for the sample (K_2NiPc) correspond to the reflexes (111) and (200) in *fcc* structure of Ni-foil [11, 18]. The lower angle peaks at $2\theta < 30°$ of pure NiPc can be found in a broadened form in the diffraction patterns of the doped sample. This means that the phthalocyanine matrix becomes progressively disordered upon doping which leads to the

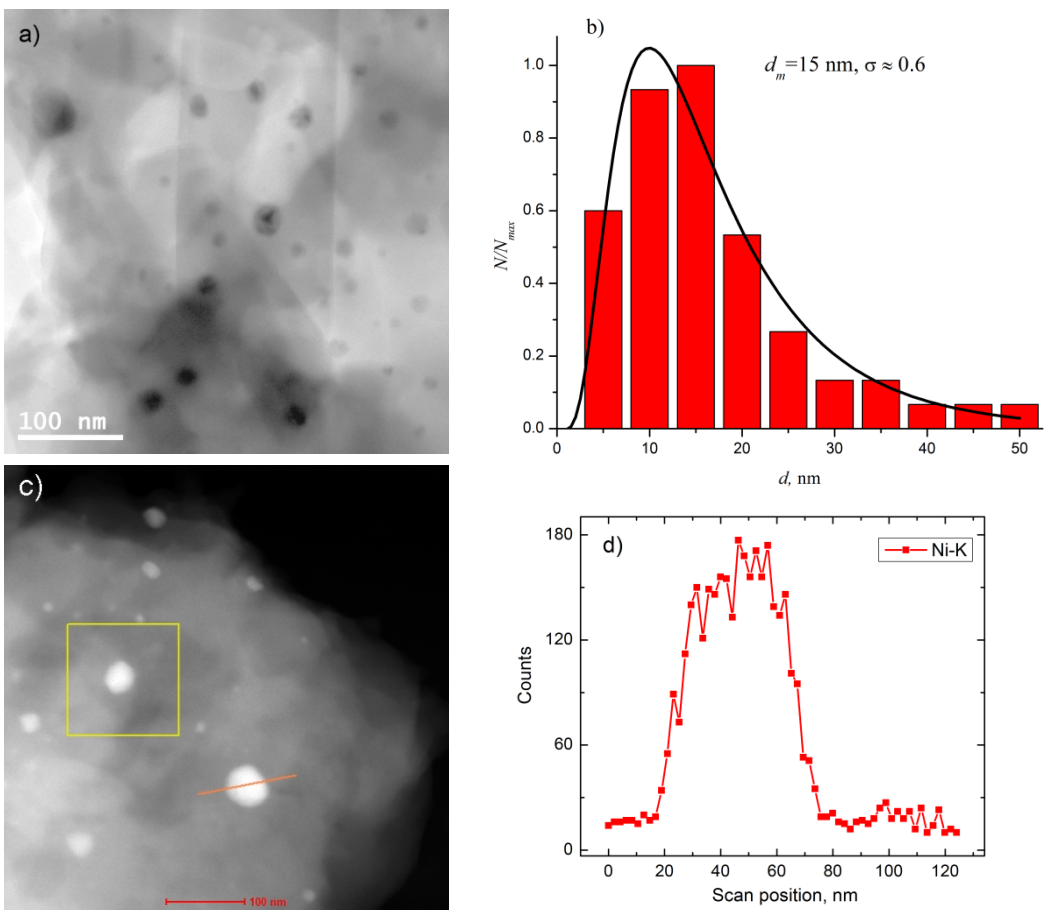

Fig. 1. TEM image of (K_2NiPc) (a) and the histogram of particle size distribution evaluated from the several TEM images (b). HAADF-STEM images of (K_2NiPc) sample (c) and EDX line-scan profile of characteristic X-ray Ni line as a function of electron probe position on the sample (d).

broadening and further, to complete disappearance of low-angle diffraction peaks. Pure NiPc has no peaks corresponding to Ni metal bonds and hence XRD data indicate that Ni nanoparticles indeed emerge upon K doping. Figure 3 shows schematically the fragment of pristine NiPc (a) and the two most plausible structural elements (b, c) which are presented in (K_2NiPc) according to TEM and XRD data.

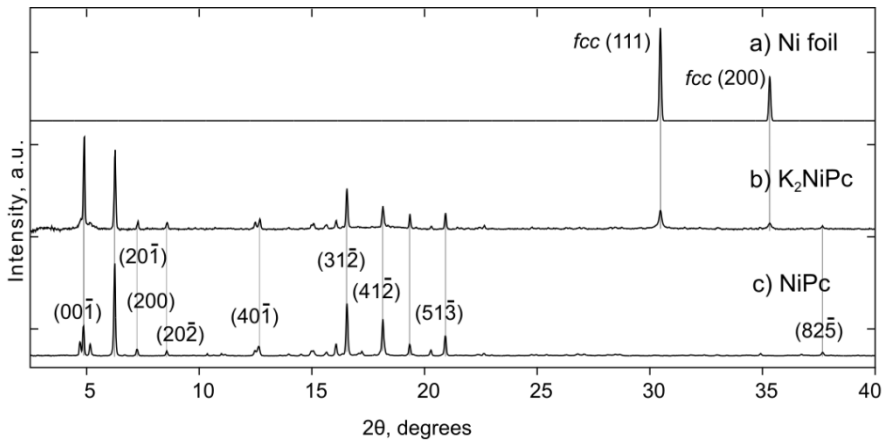

Fig. 2. Normalized XRD profiles of (a) Ni foil (simulated), (b) (K_2NiPc) (experimental) and (c) pure NiPc (experimental). X-ray wavelength is 1.072 Å.

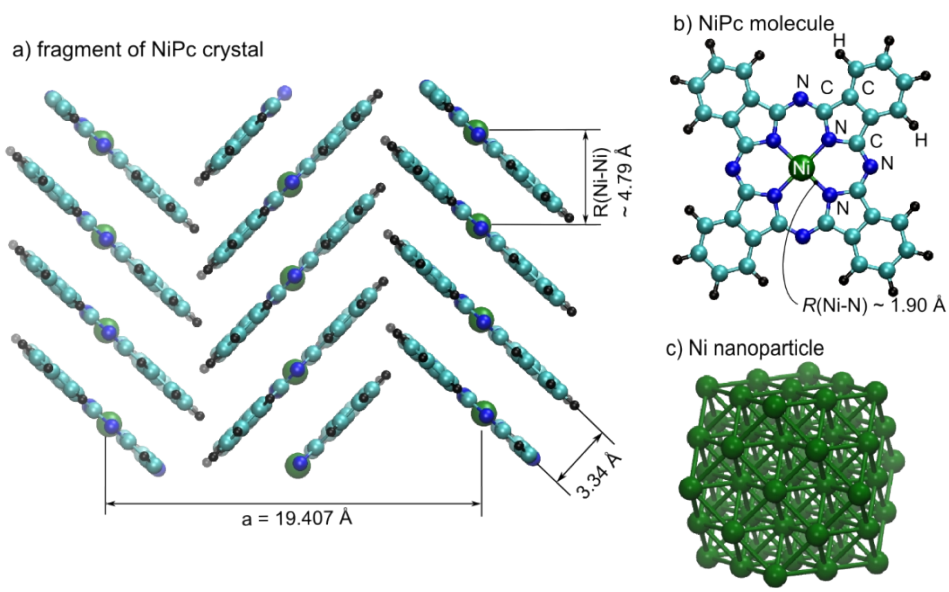

Fig.3. Schematic pictures of atomic structures of (a) the fragment of pure NiPc crystal, (b) single NiPc molecule and (c) Ni nanoparticle.

3.2. XAFS results

Quantitative characterization of the doped NiPc sample was performed using Ni K-edge XAFS. The comparison of experimental X-ray absorption near edge structures (XANES) in (K_2NiPc), pristine NiPc and in Ni foil shown in Figure 4, indicates the presence of NiPc molecules in the doped sample with no distinct evidences on the presence of Ni nanoparticles.

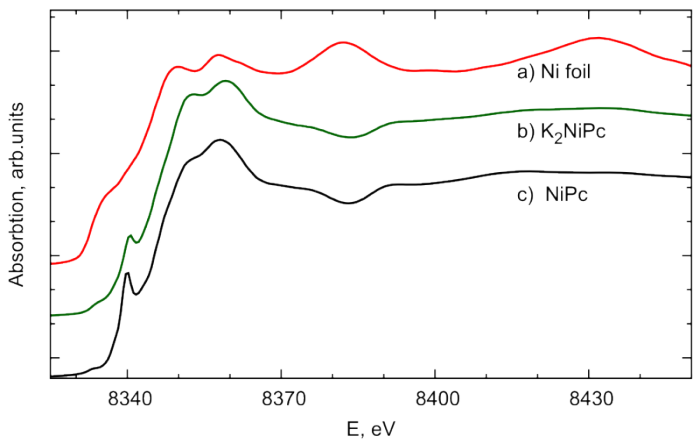

Fig. 4. Comparison of normalized experimental Ni K-edge XANES spectra in (a) Ni foil, (b) (K_2NiPc) and (c) pure NiPc.

The presence of Ni nanoparticles in the doped NiPc is distinctly observed in Figure 5, which compares the Fourier transforms (FT) $F(R)$ of oscillatory parts $\chi(k)$ of experimental Ni K-edge EXAFS in Ni-foil, (K_2NiPc) and pristine NiPc. This figure shows that $|F(R)|$ of (K_2NiPc) contains the peak corresponding to Ni-Ni interaction with interatomic distance $R_{\text{Ni-Ni}}$ close to that in the Ni-foil, while the closest Ni-Ni distance in pristine NiPc [19] is 4.79 Å which is almost 2 times larger than the Ni-Ni bond length in Ni foil (2.49 Å) [20]. This difference permits to distinguish the contributions of photoelectron scattering in Ni-nanoparticles and in NiPc molecules.

According to TEM and XRD data, the fit of $F(R)$ for Ni K-edge EXAFS in (K_2NiPc) was performed using $\chi(k)$ determined by the following expression:

$$\chi(k) = C\cdot\chi_{\text{Ni-nano}}(k) + (1 - C)\cdot\chi_{\text{NiPc}}(k) \quad (4)$$

where $\chi_{Ni\text{-}nano}(k)$ and $\chi_{NiPc}(k)$ are the contributions of Ni-nanoparticles and of NiPc molecules respectively; C – relative concentration of the absorbing Ni atoms, attributed to nanoparticles.

The distance between molecular layers in NiPc structure is about 3.5 Å (Figure 3 a) and, therefore, in the FT analysis of Ni K-EXAFS the structural model for the term $\chi_{NiPc}(k)$ in (4) included only one NiPc molecule. For pristine NiPc it was revealed [21] that to obtain agreement of theoretical $F(R)$ with the experimental one in the extended R-range (up to ~ 5.5 Å) using k_{min} ~ 2.5 Å for FT of Ni K-EXAFS one needs to account for single-scattering (SS) paths on the three nearest shells of the absorbing Ni added with three approximately linear multiple scattering (MS) paths schematically illustrated in Figure 3b. Therefore, to retain the verification of the used structural models in the extended R-range and simultaneously, to simplify these models by reducing the effect of photoelectron MS processes on the determined values of first shell's structural parameters, the fit by IFEFFIT code [22] was performed for *F(R)* obtained using FT of $k^2\chi(k)$ over the k-range $4.5 \le k \le 11.5$ Å^{-1}, in the interval $1.0 < R < 3.5$ Å.

To reveal the validity of the used scheme and to determine some nonstructural fit parameters, it was first applied to the processing of Ni K-EXAFS in the reference compounds Ni-foil and pristine NiPc (the last is one of the two basic components in eq. (4)). To decrease the number of variable parameters in the processing of Ni K-EXAFS in Ni-foil and in NiPc, the coordination numbers in the structural models for $\chi_{Ni\text{-}foil}(k)$ and $\chi_{NiPc}(k)$ were set to their crystallographic values [19, 20]. The fit of F(R) for these compounds was performed using the structural models consisting of four shells of the absorbing Ni atom in Ni-foil and of three shells – in NiPc with the following parameters for each shell to be determined: Debye-Waller (DW) parameter σ^2 and the shell's radius R. Besides, the determined parameters for Ni-foil were: the reduction factor S_0^2(Ni-foil), energy correction e_0(Ni-foil) and for NiPc: S_0^2(NiPc), e_0(NiPc) [23]. Figure 5 shows the comparison of FT magnitudes $|F(R)|$ of experimental Ni K-EXAFS with the fit results for Ni-foil and pristine NiPc and the corresponding structural parameters of the first shell of the absorbing Ni derived from EXAFS are presented in Table 1. These structural parameters are in agreement with the available XRD data. The obtained values of the DW parameters are typical for the room temperature values [24] and the values of nonstructural parameters S_0^2(Ni-foil), S_0^2(NiPc) are within their physical boundaries $0.5 \le S_0^2 \le 1.0$.

The results for Ni-foil and pristine NiPc enabled to perform structural analysis of (K_2NiPc) using eq.(4)

for the processing of Ni K-EXAFS and the values of nonstructural parameters obtained for these reference samples. The term $\chi_{Ni\text{-}nano}(k)$ in (4) included the contribution of the first shell with varied parameters $N_{Ni\text{-}Ni}$, $R_{Ni\text{-}Ni}$, $\sigma^2_{Ni\text{-}Ni}$. The term $\chi_{NiPc}(k)$ in (4) included contributions of the first three shells of the absorbing Ni atom with the variable parameters for each shell: R and σ^2. The number N of atoms in each shell was fixed to its value in pristine NiPc according to XRD data which show the presence of NiPc molecules in the doped (K_2NiPc). Concentration C was varied as the global parameter. The comparison of $|F(R)|$ of experimental Ni K-EXAFS in (K_2NiPc) with the result of the fit obtained by the described scheme based on eq.(4) is presented in Figure 5. Corresponding structural parameters of the first shells of the absorbing Ni in nanoparticles and in NiPc molecules derived from EXAFS are presented in Table 1.

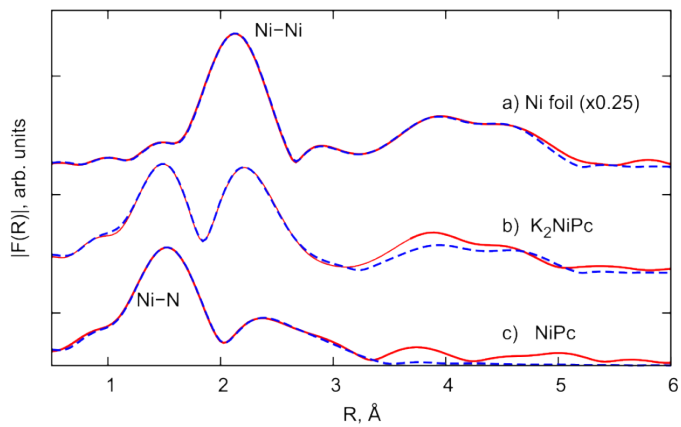

Fig. 5.Comparison of FT magnitudes $|F(R)|$ of experimental Ni K-EXAFS (solid curves) with the fit results (dashed curves) for: (a) Ni foil, (b) (K_2NiPc) and (c) pure NiPc.

The data of Table 1 show that the changes in Ni-N bond-lengths between K_xNiPc and NiPc are within error bars. Besides, for (K_2NiPc) the obtained values of DW parameters σ^2 for the first shell of Ni both in Ni nanoparticle and in NiPc molecules are reasonable for the room temperatures [24], which indicates that the used structural model based on eq.(4) takes into account the main types of local environment of the absorbing Ni atoms in this material. These results show that atomic structure of NiPc molecules is not changed significantly by doping with potassium. Nevertheless the electronic structure of NiPc could change. Another valuable result is that concentration C of Ni atoms, attributed to Ni nanoparticles in doped NiPc, is

~10 % so that the ratio NiPc:Ni is 90:10 ≈ 10:1, which is of two orders higher than for NiPc coated nanoparticles reported in [7].

Table 1. First shell structural parameters of the absorbing Ni atoms in Ni foil, (K_2NiPc) and NiPc derived from Ni K-EXAFS. The values in brackets are the reference data for Ni foil [20] and NiPc [19].

Sample	*C*, %	NiPc contribution		Ni metal contribution	
		R_{Ni-N}, Å	σ^2_{Ni-N}, Å^2	R_{Ni-Ni}, Å	σ^2_{Ni-Ni}, Å^2
Ni foil	100	–		2.49 (2.49)	0.0062
K_2NiPc	10	1.89	0.0052	2.48	0.0061
NiPc	0	1.90 (1.90)	0.0050	–	

3.3. Magnetic measurements

Here we first investigate the magnetic properties from the analyses of spectra of ferromagnetic resonance (FMR) and electron paramagnetic resonance (EPR). Figs. 6 and 7 demonstrate the first-derivative FMR and EPR spectra of (K_2NiPc) sample recorded at 8–285 K temperature range. In fact, the spectrum of the magnetic resonance at 285 K, consists of two lines: broad with the *g*-factor, $g \approx 2.15$ and narrow line with $g = 2$. The temperature behaviour of broad FMR signal in (K_2NiPc) sample is typical to single domain ferromagnetic and superparamagnetic nanoparticles [30–33]. The FMR spectra shift toward $g \approx 4$, are broadened and diminished in intensity under decreasing of temperature from room to the helium temperatures.

For comparison Fig. 6 shows also FMR spectrum of Ni nanoparticles in carbon matrix at room temperature (300 K)**.** The average diameter of Ni nanoparticles in Ni/C nanocomposite is equal to 17 nm, which is approximately equal to the sizes of nickel nanoparticles in (K_2NiPc). However, the width of the signal of FMR spectra in (K_2NiPc) samples is significantly broader than in Ni/C. The comparison of the FMR spectra of (K_2NiPc) and Ni/C suggests that the FMR in (K_2NiPc) is caused not only by nickel nanoparticles, but also by anionic NiPc molecules.

Besides the broad FMR signal in (K_2NiPc), there are also "narrow" signals at $g \approx 2$ (see Fig.6 and Fig.7). The amplitude and width of "narrow" signal of the electron paramagnetic absorption increases under decreasing the temperature from the room up to the helium temperatures. At low temperatures we resolve the two signals with line widths $\Delta H_{pp} \approx 100$ Oe and 15 Oe. The most interesting peculiarity of the "narrow" signal is the fact that the temperature dependence of its integral intensity strongly deviates from the Curie behaviour: it sharply increases as temperature decreases. The ratio of the signal I(8K)/I(280K) ≈150 is significantly different from the Curie ratio - 285/8 ≈ 35. We assume that magnetic absorption at $g \approx 2$ due to the matrix, namely by π- electrons of the anionic NiPc molecules.

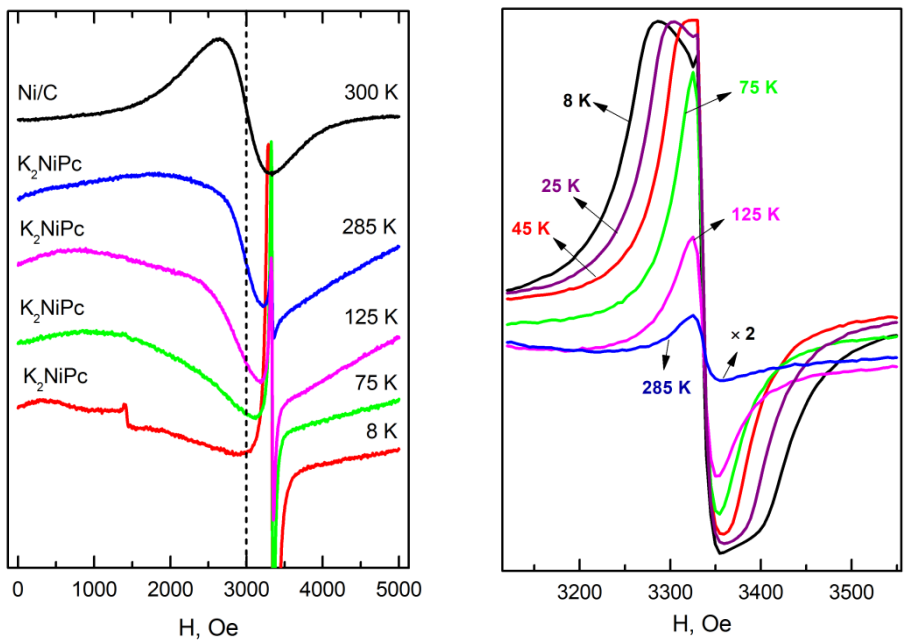

Fig.6. The spectra of magnetic resonance of (K_2NiPc) at temperatures of 285, 125, 75 and 8 K, and Ni/C nanocomposite at 293 K.

Fig.7. The ESR spectra of (K_2NiPc) sample at temperatures of 285, 125, 75, 45, 25 and 8 K.

It should be taken into account that the doping is inhomogeneous. Therefore, this results in formation not only of ferromagnetic domains due to exchange interactions between π-electrons of the anions of NiPc molecules. As a result of inhomogeneous doping, the part of the NiPc molecules remain in the diamagnetic state, while there arise also some paramagnetic centres and paramagnetic clusters consisting of molecular anions of NiPc. Under decreasing of temperature, the number of paramagnetic states and, possible, the sizes

of the clusters increase, leading to the formation of high – spin states. Apparently, high-spin states as well as orbital paramagnetism of π-electrons determines the observed a significant paramagnetism in (K_2NiPc) samples at low temperatures. In Fig. 6 at half field the absorption peak, caused by prohibited +1↔-1 transitions in triplet anions NiPc (possessing the spin S = 1) is observed at T = 8K.

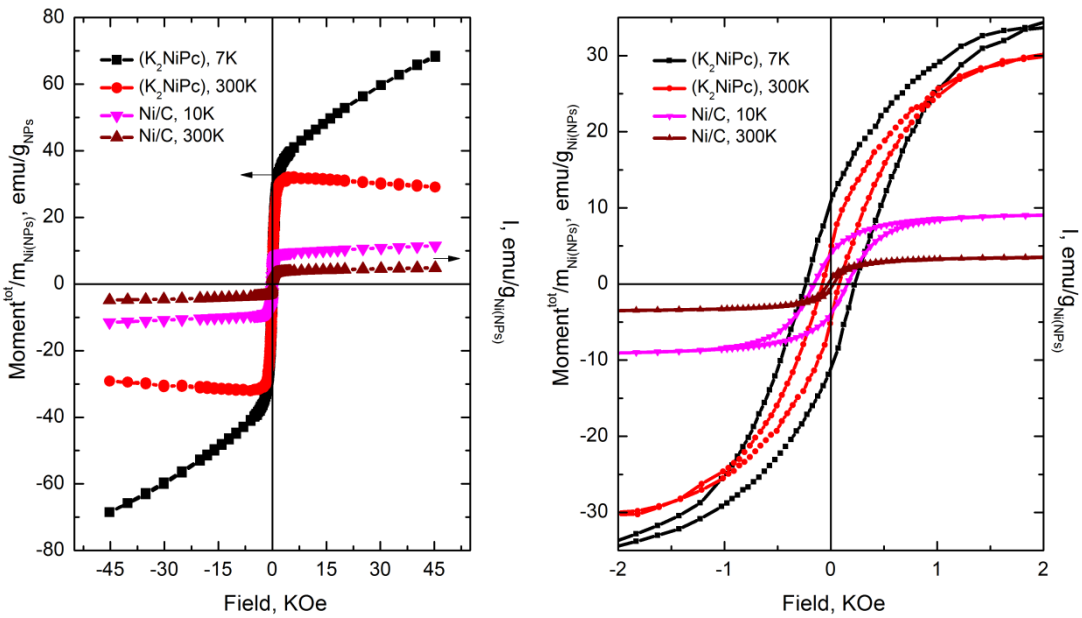

Fig.8. M_{total} / $m_{Ni\ (NPs)}$ vs. H in sample (K_2NiPc) measured at 7 K and 300 K, and the specific magnetization of nickel nanoparticles in Ni/C nanocomposites: I vs. H at T = 10 and 300K.

Fig.9. The hysteresis loops in sample (K_2NiPc) at 7 and 300K and in Ni/C nanocomposites at T = 10 and 300K.

Magnetization measurements using SQUID-magnetometer confirmed the presence of ferromagnetism and paramagnetism caused by the NiPc anion molecules. The total magnetic moment - M^{total} measured by SQUID magnetometer is a sum of ferromagnetic magnetic moments from of nickel nanoparticles and molecular NiPc anions and paramagnetic moment of the NiPc anions:

$$M^{total}(H,T) = M^{FM}_{Ni(NPs)}(H,T) + M^{FM}_{NiPc(mol)}(H,T) + \chi^{PM}_{NiPc(mol)}H \qquad (5)$$

Fig. 8 represents the dependence of M^{total} /$m_{Ni\ (NPs)}$ on H at T= 7 and 300K, where $m_{Ni\ (NPs)}$ is the mass of Ni nanoparticles in the sample. From the XAFS results, it follows that 10% of nickel in sample represents nanoparticles of Ni: in the mass ratio it is 1wt% of the mass of NiPc sample. Fig. 8 shows also comparison of the results for the specific magnetization of metallic nickel nanoparticles $I_{Ni(NPs)}$ in the nanocomposites Ni/C

having the same sizes that nanoparticles of the Ni in (K_2NiPc). Fig. 9 shows loops of magnetic hysteresis in (K_2NiPc) measured at 7 K and 300 K. These curves also sum of hysteresis loops from nanoparticles and from molecular matrices. Fig. 9 also shows for comparison the hysteresis loops in nanocomposites Ni/C at T = 10 and 300K. The analysis of results in Fig. 8 and Fig. 9 lead to the following two main conclusions:

- The magnetic moment in samples (K_2NiPc) is substantially larger than the magnetic moment of the metal Ni nanoparticles in these samples. The room-temperature ferromagnetism in (K_2NiPc) conditioned by the Ni metal nanoparticles as well as anionic NiPc molecules. However, it is difficult to get the specific magnetization of anionic NiPc molecules - I_{NiPc}^{mol}, since we do not know the fraction (amount) of molecular anions of nickel in these ferromagnetic domains.
- At the helium temperatures, besides the ferromagnetism of metal Ni nanoparticles and anionic NiPc molecules, the giant paramagnetism was detected whose contribution to the total magnetization at H = 45 kOe comparable and even more than ferromagnetic one. This paramagnetism strongly depends on the temperature and practically disappear at the room temperature by analogy with the "narrow" signal in the EPR measurements. Obviously, this paramagnetism results due to the presence NiPc anions and clusters of molecular NiPc anions.

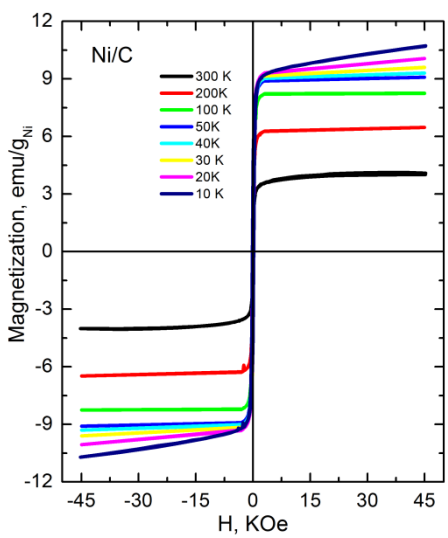

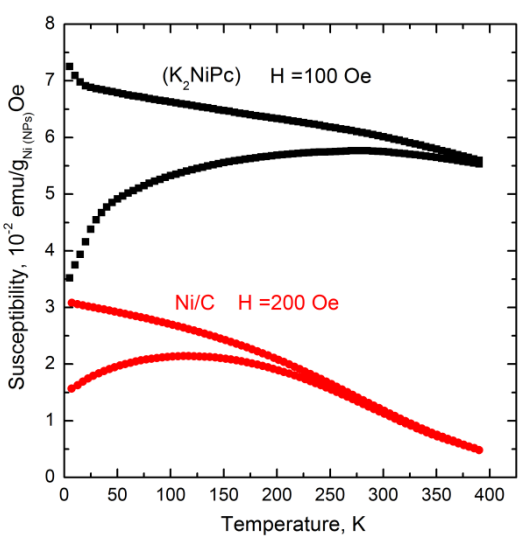

Fig.10. M vs. H in Ni/C at temperatures 10, 20, 30, 40, 50, 100, 200 and 300K

Fig.11. ZFC / FC susceptibility curves in (K_2NiPc) and Ni/C at 100 Oe and 200 Oe.

Because of wide distribution of nanoparticles in (K_2NiPc) it is necessary to consider the effect of superparamagnetic nanoparticles at SQUID measurements. It is impossible to exclude effect of superparamagnetism from anionic NiPc molecules also. Figure 10 provides the dependences of M vs. H at different temperatures in Ni/C samples. It is apparent that at low magnetic field (<1000 Oe), under the decreasing temperature the magnetization increases drastically since it is accompanied with the transition of superparamagnetic nanoparticles to blocked ferromagnetic state. The magnetization increase ≈ 6 emu/g and it is approximately equal to increase of the magnetization in (K_2NiPc) (see Figs. 8 and 9). Fig.11 introduces ZFC/FC susceptibility curves in (K_2NiPc) and Ni/C at magnetic fields 100 Oe and 200 Oe. For nanoparticles nickel in Ni/C, this figure confirms the presence of broad size distribution having the average blocking temperature equal to 110K. From this figure, it is also seen that contribution of superparamagnetism in the (K_2NiPc) sample is insignificant.

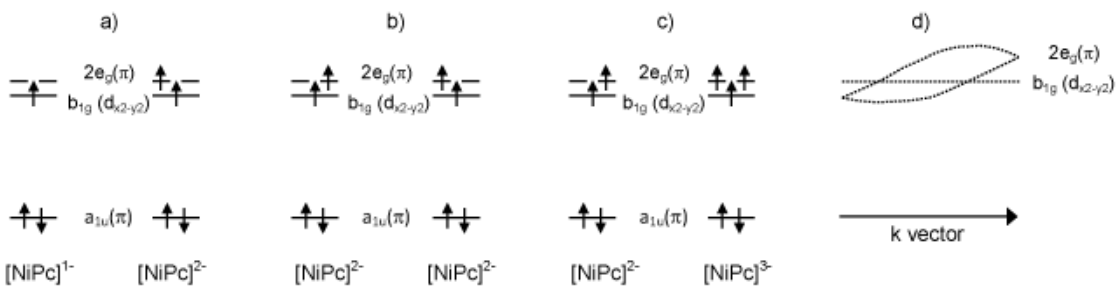

Fig.12. Scheme of valence molecular orbitals of NiPc anions at x=1.5 (a), x=2 (b), x=2.5 (c), and fragment of one-dimensional band structure of NiPc (d).

In order to understand the magnetism of molecular NiPc anions, we consider energy levels of the NiPc molecules [25]. Fig. 12 demonstrates scheme of valence molecular orbitals of adjacent NiPc anions at = 1.5; 2 and 2.5; and the fragment of NiPc band structure [26, 27]. The schemes a) and b) are very similar to the valence band metal nickel ($3d^9 4s^1$). In the case of (K_2NiPc) the π-electrons play a role of conduction electrons. In reality, optimally doped MPc samples reveal metallic conductivity [28]. In the scheme c), corresponding to π^1–π^2, the mechanism of double exchange is also essential in analogy with inorganic magnetic dimers (d^1–d^2) [29]. The delocalization of an "extra" electron between adjacent molecular anions leads to their ferromagnetic ordering. It should be noted that stabilization of the ferromagnetic state due to

the double exchange is much stronger than the Heisenberg stabilization [29, 8, 10].

Conclusion

The technique of intercalation of potassium vapours into polycrystalline powders of NiPc at relatively low temperatures (~300°C) was developed. HRTEM analysis showed that in (K_2NiPc) samples the metallic nanoparticles are formed with a mean diameter of ~ 15 nm. Comparison of XRD patterns in pristine NiPc, (K_2NiPc) and nickel foil showed the presence of nickel nanoparticles with *fcc* structure in the inner region of particle and the disordering in mutual orientation of different NiPc molecules under the preserved structure of each molecule. Atomic concentration of Ni nanoparticles in (K_2NiPc) matrix obtained from EXAFS data is 10%. FMR spectroscopy showed that total ferromagnetic absorption is composed not only by Ni nanoparticles but there is a significant contribution from the doped molecular matrix of NiPc. At helium temperatures, along with the observed ferromagnetic resonance of metal Ni nanoparticles and anion NiPc molecule, at $g = 2$ we observed also the giant paramagnetism with drastic decrease of intensity with the temperature. EPR signal at $g = 2$, apparently is determined by NiPc anions and clusters of molecular NiPc anions. Magnetization measurements using SQUID-magnetometer also confirm that the room-temperature ferromagnetism in the samples (K_2NiPc) is determined by the nickel nanoparticles and contribution of matrix caused by the anions of NiPc molecules.

Acknowledgements

The authors thank G. Asatryan for his support in conducting the magnetic resonance measurements. This work was supported by the RA MES State Committee of Science and Russian Foundation for Basic Research (RF) in the frames of the joint research projects SCS 15RF-085 and RFBR 15-52-05051 respectively, and by the grant of Volkswagen Stiftung project N A108857.

References

1. P. Modisha, T. Nyokong, Fabrication of phthalocyanine-magnetic nanoparticles hybrid nanofibers for degradation of Orange-G, Journal of Molecular Catalysis A: Chemical 381 (2014) 132–137, http://dx.doi.org/10.1016/j.molcata.2013.10.012

2. XueYan Wang, JianBang Zheng, Kai Qiao, JunRong Qu, ChongDe Cao, Studies on structure and Raman spectroscopy of Ni-doped copper phthalocyanine thin films, Applied Surface Science 297 (2014) 188-194. http://dx.doi.org/10.1016/j.apsusc.2014.01.122

3. M. Idowu and T. Nyokong, Photophysical behavior of fluorescent nanocomposites of phthalocyanine linked to quantum dots and magnetic nanoparticles, Int. J. Nanosci. 11 (2012) 1250018.

4. J. G. Guan, W. Wang, R. Z. Gong, R. Z. Yuan, L. H. Gan, and K. C. Tam, One-step synthesis of cobalt-phthalocyanine/iron nanocomposite particles with high magnetic susceptibility, Langmuir 18 (2002) 4198-4204.

5. Antunes E., Rapulenyane N., Ledwaba M., Litwinski C., Chidawanyika W., Nyokong T. The synthesis and characterisation of magnetic nanoparticles and their interaction with a zinc phthalocyanine Inorg. Chem. Commun. 29 (2013) 60-64 http://dx.doi.org/10.1016/j.inoche.2012.12.010

6. S. Sanvito, Molecular spintronics, Chemical Society Reviews, 40 (2011) 3336-3355, DOI: 10.1039/C1CS15047B

7. B. Brauer, Y. Vaynzof, W. Zhao, A. Kahn, W. Li, D. R. T. Zahn, C. de Julian Fernandez, C. Sangregorio, and G. Salvan, Electronic and magnetic properties of Ni nanoparticles embedded in various organic semiconductor matrices, J. Phys. Chem. B 113 (2009) 4565-4570.

8. E.G. Sharoyan, A.S. Manukyan, High Temperature Molecular Magnetism Caused by π-Electrons: Copper Phthalocyanine Doped with Alkaline Metals, J. Porphyrins and Phthalocyanines 9 (2005) 846-851.

9. A.R. Harutyunyan, L.S. Grigoryan, E.G. Sharoyan, Preparation and magnetic properties of zinc phthalocyanines homogeneously doped with alkaline metals, Materials Science 14 (1988) 121. DOI: 10.3103/S1068337208040075

10. Sharoyan E.G., Sharoyan V.E., Ovsyannikov P.M. EXAFS Studies of Organic Molecular Ferromagnets Based on Cobalt Phthalocyanine: Na2.8CoPc J. Porphyrins Phthalocyanines 02 (1998) 237-241.

11. A. Manukyan, A. Mirzakhanyan, L. Sajti, R. Khachaturyan, E. Kaniukov, L. Lobanovsky, E. Sharoyan, Magnetic Properties of Carbon-Coated Ni Nanoparticles Prepared by Solid-Phase Pyrolysis of Nickel-Phthalocyanine, NANO, 10 (2015) 1550089-1.

12. F. Moser, A. Thomas. Phthalocyanine compounds, Monograph series (Reinhold Pub. Co., 1963) p. 365.

13. R. Taube. Zur Elektronenstruktur anionisher Phthalocyaninkomplexe einiger 3d-Elemente, Z. Chemie Z. Chem. 6 (1966) 8-21.

14. A.N. Sidorov, Optika i spektroskopiya 40 (1976) 492.

15. J. Simon, J.-J. Andre. Molecular Semiconductors, Springer-Verlag, Berlin-Heidelberg (1985).

16. A.R. Harutyunyan, L.S. Grigoryan, E.G. Sharoyan. Magnetic Properties of Free-Base Phthalocyanine Doped with Sodium, Phys. Stat. Sol. 142 (1987) 169-172.

17. J. Mack, M.J. Stillman, Assignment of the Optical Spectrum of Metal Porphyrin and Phthalocyanine Radical Anions, J. Porphyrins and Phthalocyanines 5 (2001) 67-76.

18. Manukyan A., Mirzakhanyan A., Badalyan G., Shirinyan G., Fedorenko A., Lianguzov N., Yuzyuk Y., Bugaev L., Sharoyan E. Nickel nanoparticles in carbon structures prepared by solid-phase pyrolysis of nickel-phthalocyanine, J. Nanopart. Res. Springer Netherlands 14 (2012) 1-7

19. N. B. McKeown, Phthalocyanine Materials: Synthesis, Structure and Function (Cambridge University Press, 1998) P. 211.

20. A. Chichagov, D. Varlamov, R. Dilanyan, T. Dokina, N. Drozhzhina, O. Samokhvalova, T. Ushakovskaya, Mincryst: A crystallographic database for minerals, local and network (www) versions, Crystallogr. Rep. 46 (2001) 876–879.

21. N.A. Kolpacheva, L.A. Avakyan, A.S. Manukyan, A.A. Mirzakhanyan, E.G. Sharoyan, V.V. Pryadchenko, Y.V. Zubavichus, A.L. Trigub, A.G. Fedorenko, L.A. Bugaev, Synthesis and Investigation of the Structure of Nanocomposites Based on Nickel Nanoparticles Dispersed in a Phthalocyanine Matrix, Phys. Solid State 58 (2016) 1004-101.

22. B. Ravel, M. Newville, Athena, artemis, hephaestus: data analysis for x-ray absorption spectroscopy using ifeffit, J. Sync. Rad. 12 (2005) 537-541.

23. D. Koningsberger, R. Prins, X-ray absorption: principles, applications, techniques of EXAFS, SEXAFS, and XANES, Chemical analysis (Wiley, New York, 1988) p. 688.

24. A. V. Poiarkova, J. J. Rehr, Multiple-scattering x-ray-absorption fine-structure debye-waller factor calculations, Phys. Rev. B 59 (1999) 948-957.

25. A. Rosa, E.J. Baerends, Origin and relevance of the staggering in one-dimensional molecular metals. A density functional study of metallophthalocyanine model dimers, Inorg. Chem. 31 (1992) 4717-4726.

26. Kutzler F.W., Ellis D.E., A comparison of the one-dimensional band structures of Ni tetrabenzoporphyrin and phthalocyanine conducting polymers, J. Chem. Phys. 84 (1996) 1033-1038.

27. Liao M.-S., Scheiner S. Electronic structure and bonding in metal phthalocyanines, Metal=Fe, Co, Ni, Cu, Zn, Mg, J. Chem. Phys. 114 (2001) 9780-9791.

28. M. F. Cracium, S. Rogge, A.F. Morpurgo, Correlation between molecular orbitals and doping dependence of the electrical conductivity in electron-doped metal-phthalocyanine compounds, J. Am. Chem. Soc. 127 (2005) 12210.

29. J.J. Borras-Almenar, E. Coronado, B.S. Tsukerblat, R. Georges, Lokalization vs delocalization in molecules and clusters: electronic and vibronic interactions in mixed valence systems, in: E. Coronado, P. Delhaes, D. Gatteschi, J.S. Miller (Eds.), Molecular Magnetism: From Molecular Assemblies to the Devices, NATO ASI Series E, Kluwer Academic Publishers, Dordrecht, The Netherlands, 1996, pp. 105-139.

30. R. Berger, J.-C. Bissey, J. Kliava, H. Daubric, C. Estournes, Temperature dependence of superparamagnetic resonance of iron oxide nanoparticles, J. Magn. Magn. Mater. 234 (2001) 535-544.

31. R. Berger, J.-C. Bissey and J. Kliava, Lineshapes in magnetic resonance spectra J. Phys.: Condens. Matter., 2000, **12**, 9347.

32. V. N. Krivoruchko, A. I. Marchenko, and A. A. Prokhorov, Superparamagnetic resonance of single-domain nanoparticles of $LaSrMnO_3$. LOW TEMPERATURE PHYSICS, 33 (2007) 433-438.

33. V. Singh, M. S. Seehra, F. E. Huggins, N. Shah, and G. P. Huffman, Temperature and size deoendence of magnetic and electron magnetic resonance of Fe nanoparticles embedded in amorphous SiO_2 matrix, J. Appl. Phys. 109, (2011) 07B506-1 – 07B506-3.

Highlights

A method of K atoms intercalation into nickel phthalocyanine (NiPc) matrix was implemented.

Formation of Ni nanoparticles and a magnetic nickel phthalocyanine anions matrix has been developed.

Structure, morphology and magnetic properties of K_2NiPc sample were investigated.

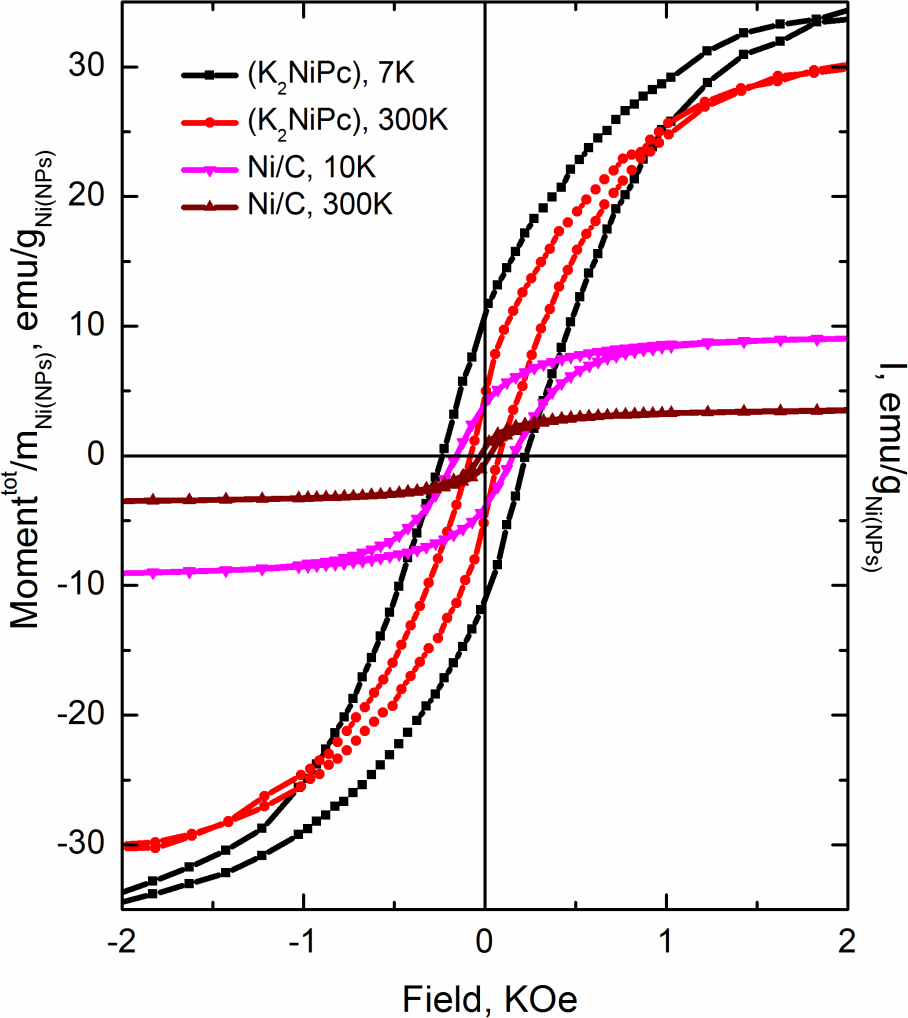
(K2NiPc), 7K
(K2NiPc), 300K
Ni/C, 10K
Ni/C, 300K
Moment^tot/m_Ni(NPs), emu/g_Ni(NPs)
I, emu/g_Ni(NPs)
Field, KOe
30
20
10
0
-10
-20
-30
-2
-1
0
1
2

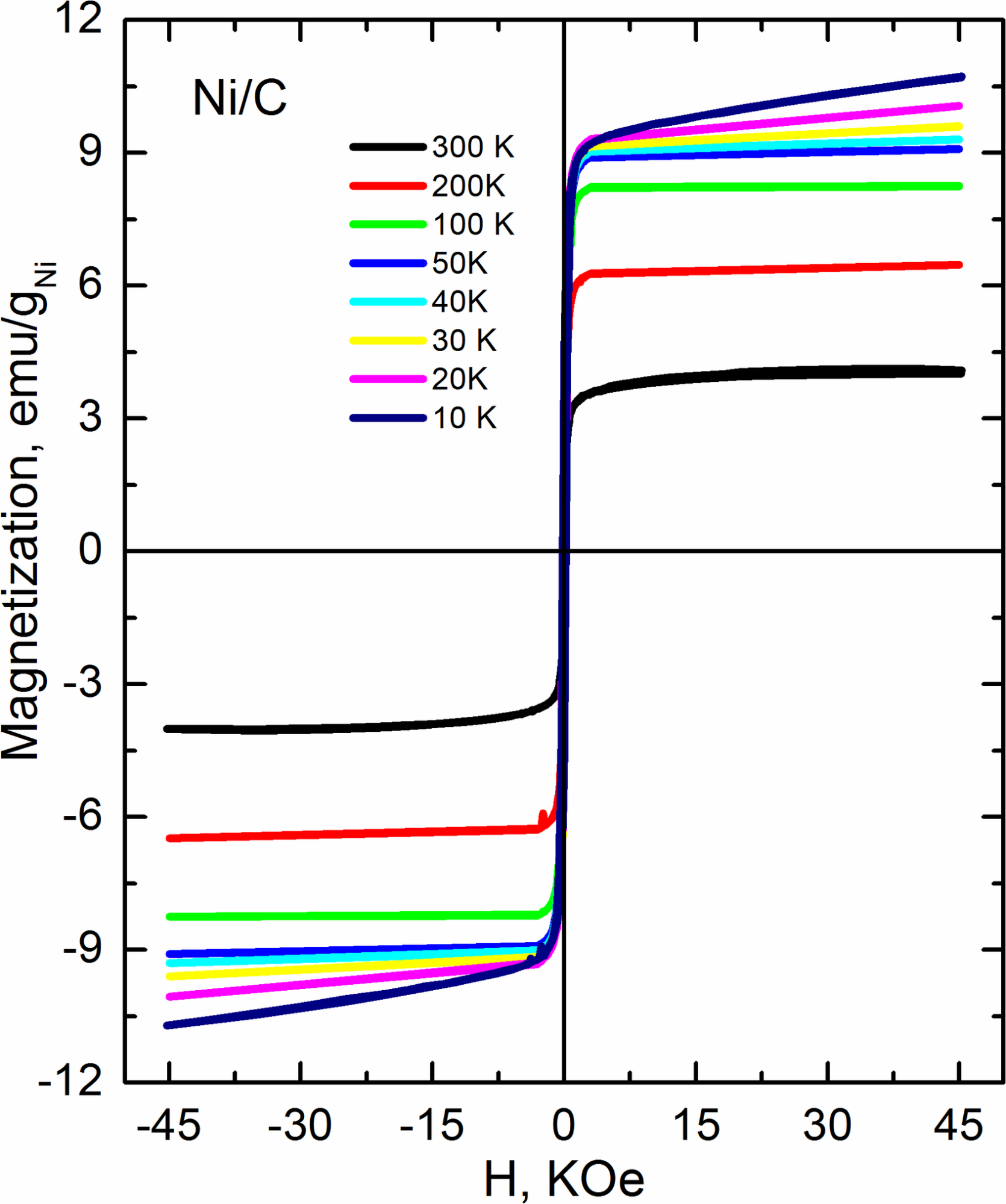
Ni/C
300 K
200K
100 K
50K
40K
30 K
20K
10 K
Magnetization, emu/g$_{Ni}$
H, KOe
12
9
6
3
0
-3
-6
-9
-12
-45
-30
-15
0
15
30
45

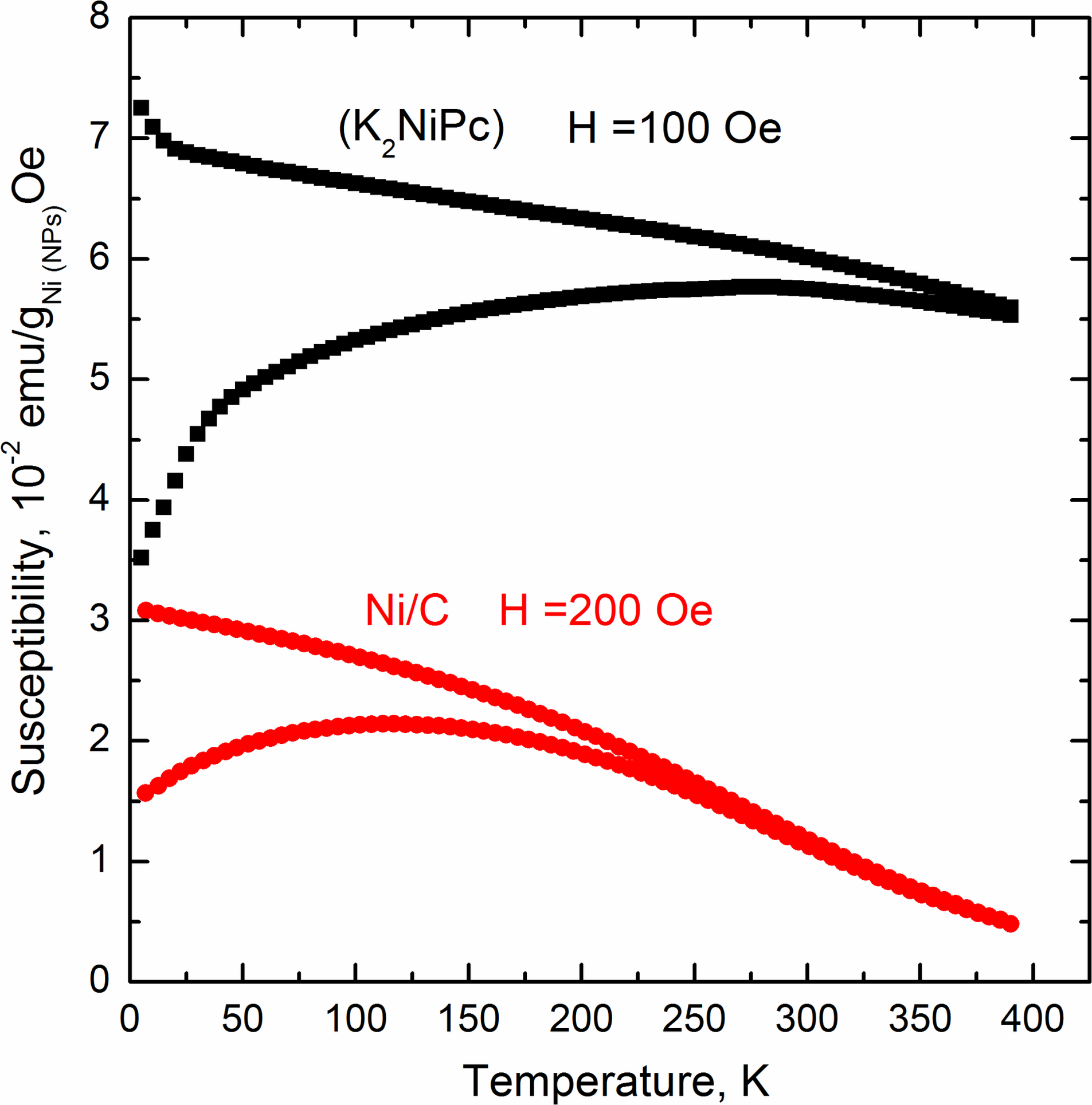
(K2NiPc) H =100 Oe
Ni/C H =200 Oe
Susceptibility, 10-2 emu/gNi (NPs)Oe
Temperature, K
0
1
2
3
4
5
6
7
8
0
50
100
150
200
250
300
350
400

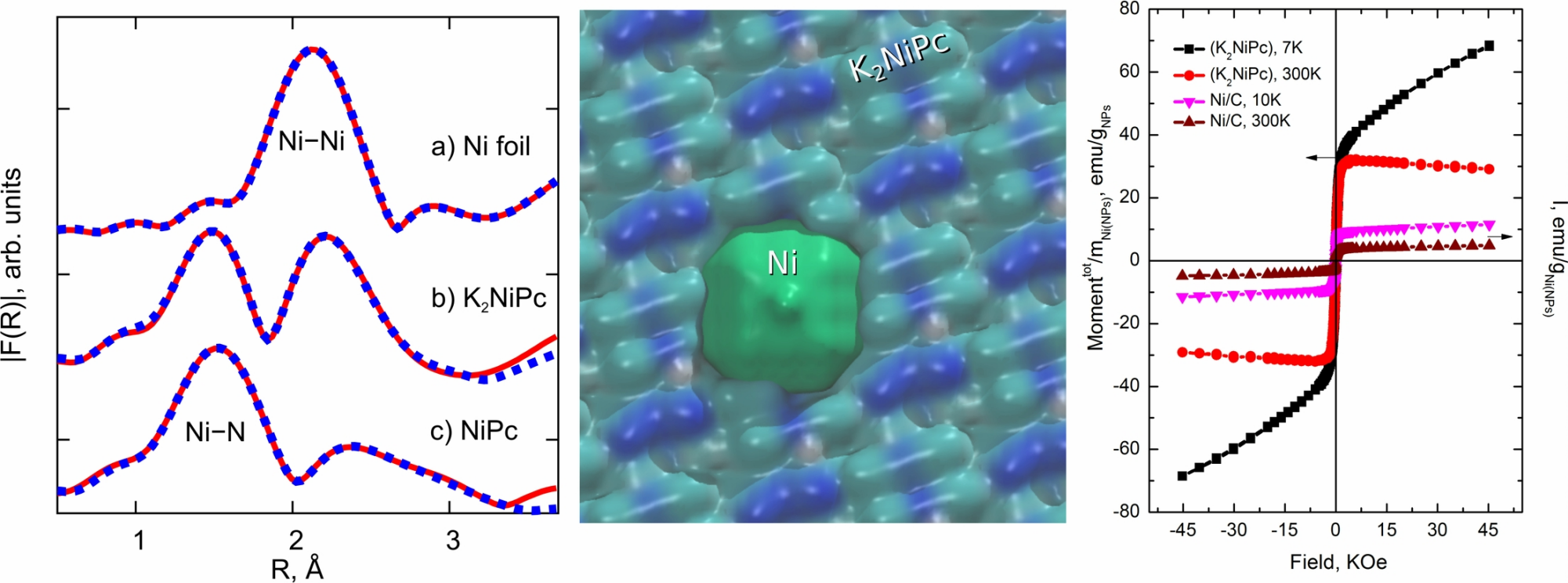
|F(R)|, arb. units
Ni–Ni
a) Ni foil
b) K2NiPc
Ni–N
c) NiPc
1
2
3
R, Å
K2NiPc
Ni
(K2NiPc), 7K
(K2NiPc), 300K
Ni/C, 10K
Ni/C, 300K
Moment^tot/m_Ni(NPs), emu/g_NPs
I, emu/g_Ni(NPs)
80
60
40
20
0
-20
-40
-60
-80
-45
-30
-15
0
15
30
45
Field, KOe